CERN - EUROPEAN ORGANIZATION FOR NUCLEAR RESEARCH

Submitted to
Topical Conference on
Baryon Resonances
Oxford, 5-7 July 1976

CERN/EP/PHYS 76-40
30 June 1976

THE K^-n ELASTIC DIFFERENTIAL CROSS SECTION BETWEEN 1.2 AND 2.2 GeV/c

P. Baillon, C. Bricman, Y. Déclais, J. Duchon, M. Ferro-Luzzi, M. Louvel, J.P. Patry, J.M. Perreau, J. Séguinot and T. Ypsilantis

CERN-Caen Collaboration

ABSTRACT

This counter experiment used a liquid deuterium target associated with a neutron detector, a magnetic spectrometer and a system of veto counters which rejected the inelastic events. It was performed in a low energy K^- beam at the CERN PS. From the analysis of the $K^-d \to K^-np$ reactions where the proton is slow enough to be considered as a spectator we extracted the $K^-n \to K^-n$ elastic cross section for most of the c.m. angular range and for a K^-n c.m. energy going from 1.85 to 2.3 GeV. The effects due to the Fermi momentum were taken into account. Corrections due to internal double scattering were evaluated through a Monte-Carlo program and applied to the data. A phase shift analysis of these new data together with all the K^-p available data in the energy range has been done.

PB/gf

1. EXPERIMENTAL PROCEDURE

This experiment will be fully described in a forthcoming publication [1]. The lay-out is shown in fig. 1. Briefly, the experimental set-up can be summarised as follows.

The incident particle was coming from a low-energy partially separated K^- beam. The final identification was done by a threshold Cerenkov counter. The target, 25 cm long and 6 cm in diameter, was filled with liquid deuterium. A veto-box surrounding the target was made of scintillator lead sandwiches and detected all charged particles as well as γ rays coming from π^o decays. Slits and holes in this veto-box were introduced to let the desired particles of the K^-np final state reach the corresponding detectors. The veto box is indicated on fig. 1 as "coque" (B_1, B_2 and B_3). Two arms of detectors measured the outgoing particles.

The first (neutral branch) consists of two XY multiwire proportional chambers followed by a neutron detector. This neutron detector was made of 18 converter plates interleaved with optical spark chambers. The sparks were looked at by two plumbicon cameras and their position digitized before being recorded on tape. The two XY proportional chambers were used to measure also events with outgoing protons. The acceptance of the chambers was matched to the neutron detector acceptance.

The other arm (charged branch) was a magnetic spectrometer made of three multiwire proportional chambers, two XY and one U, in front of a large aperture C-magnet. The magnet was followed by two other XY proportional chambers. This arm measured the direction and momentum of the scattered K.

The trigger was determined by a set of scintillator counters. In fig. 1, these counters are labelled S_1, S_2, for the incident particle, S_3, S_4, S_5 for the charged branch, and S_6, S_7 for the neutral branch; S_{tr} defined a non-interacting K^-.

Two kinds of triggers were defined:

(i) The K^-n trigger, corresponding to the reaction $K^-d \to K^-n(p_s)$ where the proton had an energy less than 200 MeV/c and did not escape the target. This trigger was defined as $(S_1S_2)\cdot(\bar{B}_1\bar{B}_2\bar{B}_3)\cdot(\bar{S}_{tr}\bar{S}_3\bar{S}_4\bar{S}_5\bar{S}_6)$.

(ii) The K^-p trigger, corresponding to the reaction $K^-d \to K^-p(n_s)$ where the proton was energetic enough to go through the liquid hydrogen. The trigger was defined as $(S_1S_2)\cdot(\bar{B}_1\bar{B}_2\bar{B}_3)\cdot(\bar{S}_{tr}\bar{S}_3\bar{S}_4\bar{S}_5\bar{S}_7)$.

In both cases we measure the momentum and the direction of the incident and outgoing K^- plus the direction of the outgoing nucleon (neutron or proton). The veto-box rejects events with extra particles. With this rejection we are left only with K^-np final states and the measurement leads to a zero constraint fit which allowed us to reconstruct completely the kinematics of each event.

2. DETERMINATION OF THE CROSS SECTIONS

2.1 Rejection of residual inelastic events

We reject the residual inelastic events, where the extra particle escaped the veto-box, by imposing cuts on the recorded events. Because we are interested only in events with slow (spectator) nucleon, the two outgoing particles of a good event should have a kinematical configuration close to that of an elastic event on a free nucleon. Coplanarity cuts and missing mass cuts broadened by the Fermi momentum are therefore possible. We thus reduced the inelastic contamination to less than 2%.

2.2 Acceptance calculation

A Monte-Carlo program evaluated the geometrical acceptance of the apparatus. We determined experimentally the efficiency of the neutron detector by taking together with the K^- events a large number of $\pi^-d \to \pi^-pn$ events. By demanding that the proton does not leave the target we restrict the sample to events with slow protons (spectator).

The direction and the momentum of the neutron is then rather well defined by the measurement of the outgoing π^-. The ratio between the number of visible neutrons and the total number of neutrons crossing the detector determines the efficiency of the neutron detector (fig. 2).

2.3 Deuterium effects

In order to extract the K^-n or K^-p cross section, we have to take into account the effects due to the binding energy of the deuteron, generally called Fermi-momentum corrections. The first is a flux correction taking into account the variation of the relative velocity of the interacting nucleon and the incident K^-, the second is a shift in mass and angle with respect to the free nucleon reaction. The two corrections are easily done because the events are fully measured.

To reduce the ambiguity (target or spectator) between the two nucleons, we demanded the non-interacting nucleon to have a momentum less than 200 MeV/c and the interacting one to have a momentum larger than 400 MeV/c. A Monte-Carlo program calculated the corrections to be applied to compensate for those cuts. The same program evaluated, using known $\bar{K}N$ phase shift, the remaining contribution of events coming from the unwanted interacting nucleon.

We are now left with more complicated corrections due to the interaction of the outgoing particles with the other nucleon. These corrections are the double-scattering corrections and are summarised in the three following diagrams.

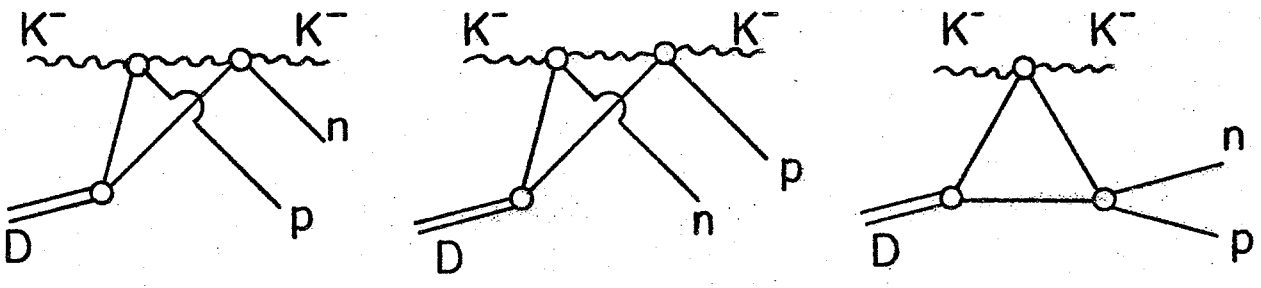

Following the method indicated in ref. [2], the contribution of the three diagrams were evaluated using the available $\bar{K}N$ and NN phase shifts [3 and 4]. The corrections are important only in the forward region and for the low energy part of the experiment. These corrections are mainly due to nucleon-nucleon rescattering and may reach $\sim$ 30% but are generally below 10% for most of the angular range. These corrections were applied only for energies below 2200 MeV where $\bar{K}N$ phase shifts are available. We use the RLIC 76 [3] phase shifts. In fig. 3 we compare the expected differential K^-p elastic cross sections obtained using the RLIC 76 and Hemingway 75 phase shifts [3, 5] with the measured K^-p sections from our $K^-p(n_s)$ corrected as indicated above. The good agreement between the measurements and the predictions gives confidence in the procedures used.

In fig. 4 we display the same comparison for the K^-n elastic cross sections. We notice good agreement in the low energy region with the RLIC 76 prediction. At higher energy RLIC 76 shows oscillations which are not in our data. We also notice a consistently poor agreement with the Hemingway 75 predictions.

3. PHASE SHIFT ANALYSIS

Using a technique similar to that of Hemingway 75 we performed a phase shift analysis. Starting from values close to Hemingway 75, we found a new minimum giving a good fit to all the K^-p, K^0n and K^-n data resulting in a slight change of the resonance parameters and a modification of the background mainly for the low partial waves. The χ^2 for the fit with 114 parameters was 2929, the expected χ^2 being 2150. Fig. 5 shows the Argand diagrams of this solution. Fig. 6 shows the K^-n angular distribution compared with the results of the fit. Fig. 7 shows the K^-p and $\bar{K}^0n$ data compared to the fit.

In some regions there is poor agreement between the predictions of the fit and the expansion in associated Legendre polynomials. This is

due to the fact that for most of the energies the polarization was not measured over the whole angular range, thereby making these expansions not very reliable. For these energies we have used directly the measured polarization.

REFERENCES

[1] Y. Declais et al., to be submitted to Nucl. Physics B.

[2] L. Bertocchi and A. Cappella, Nuovo Cim. 51A (1967) 369.
E. S. Abers et al., Nuovo Cim. 42A (1966) 363.
P. Baillon, CERN/D.Ph.II/PHYS 72-50, unpublished (1972).

[3] G. P. Gopal et al., Rutherford Lab. 75-182 (PR PNT).

[4] H. MacGregor et al., Phys. Rev. 182 (1969) 1714.

[5] R. Hemingway et al., Nucl. Physics. B91 (1975) 12.

FIGURE CAPTIONS

Fig. 1 Lay-out of the experiment.

Fig. 2 Efficiency of the neutron counter. Open circles correspond to polyethylene converters, black points to iron converters in two different conditions.

Fig. 3 (a-c) K^-p differential cross section from $K^-p(n_s)$ compared to the RLIC 76 and the Hemingway 75 predictions.

Fig. 4 (a) K^-n differential cross sections compared to the RLIC 76 predictions and the Hemingway 75 predictions.

(b) K^-n differential cross section not corrected for double scattering.

Fig. 5 (a-b) Argand diagrams for the present phase shift analysis. Points are give every 0.036 GeV/c. Starting value 1.1 GeV/c, final value 2.0 GeV/c (H).

Fig. 6 K^-n differential cross sections compared to the predictions of our analysis.

Fig. 7 (a) K^-p Legendre polynomial coefficients compared to the predictions of our analysis.

(b) Same as above for associated Legendre polynomial coefficients.

(c) Same as above for the $\bar{K}^0n$ Legendre polynomial coefficients.

Fig. 8 Total cross sections and ratios Ref(o)/Imf(o) compared to the predictions of our analysis.

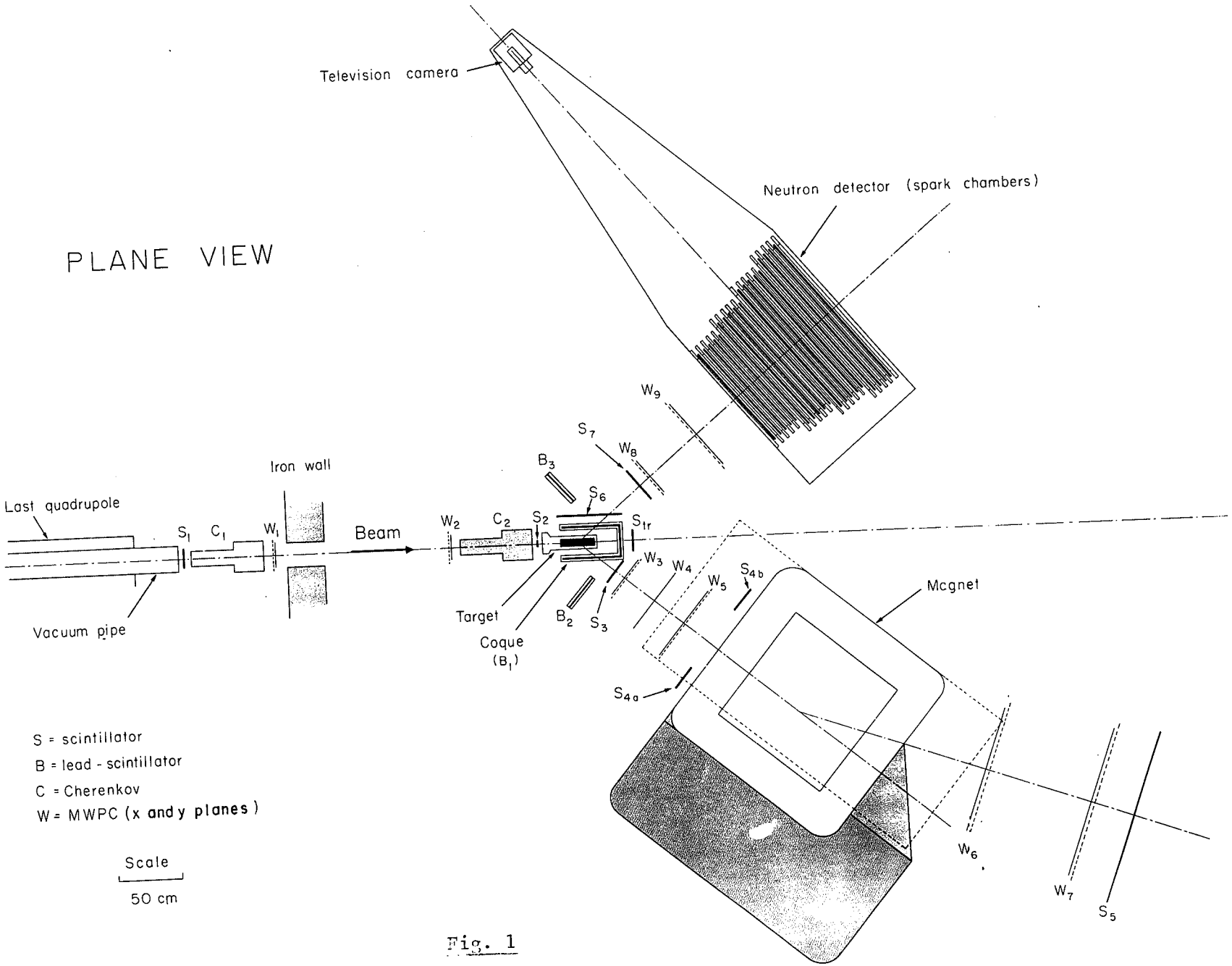
PLANE VIEW
Television camera
Neutron detector (spark chambers)
Iron wall
Last quadrupole
Beam
Vacuum pipe
Target
Coque
(B1)
Mcgnet
S = scintillator
B = lead - scintillator
C = Cherenkov
W = MWPC (x and y planes)
Scale
50 cm

Fig. 1

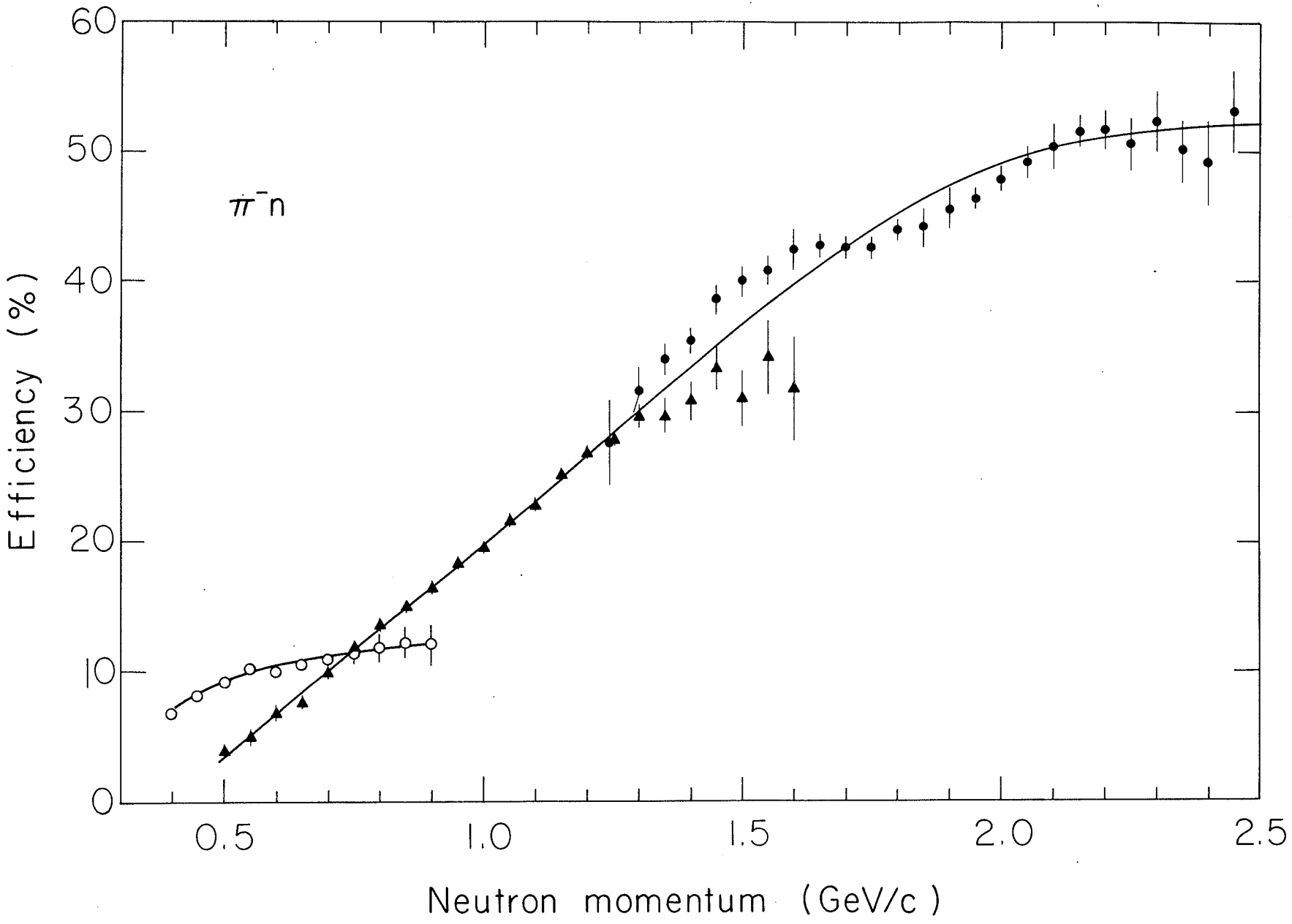
60
50
40
30
20
10
0
π^-n
Efficiency (%)
0.5
1.0
1.5
2.0
2.5
Neutron momentum (GeV/c)

Fig. 2

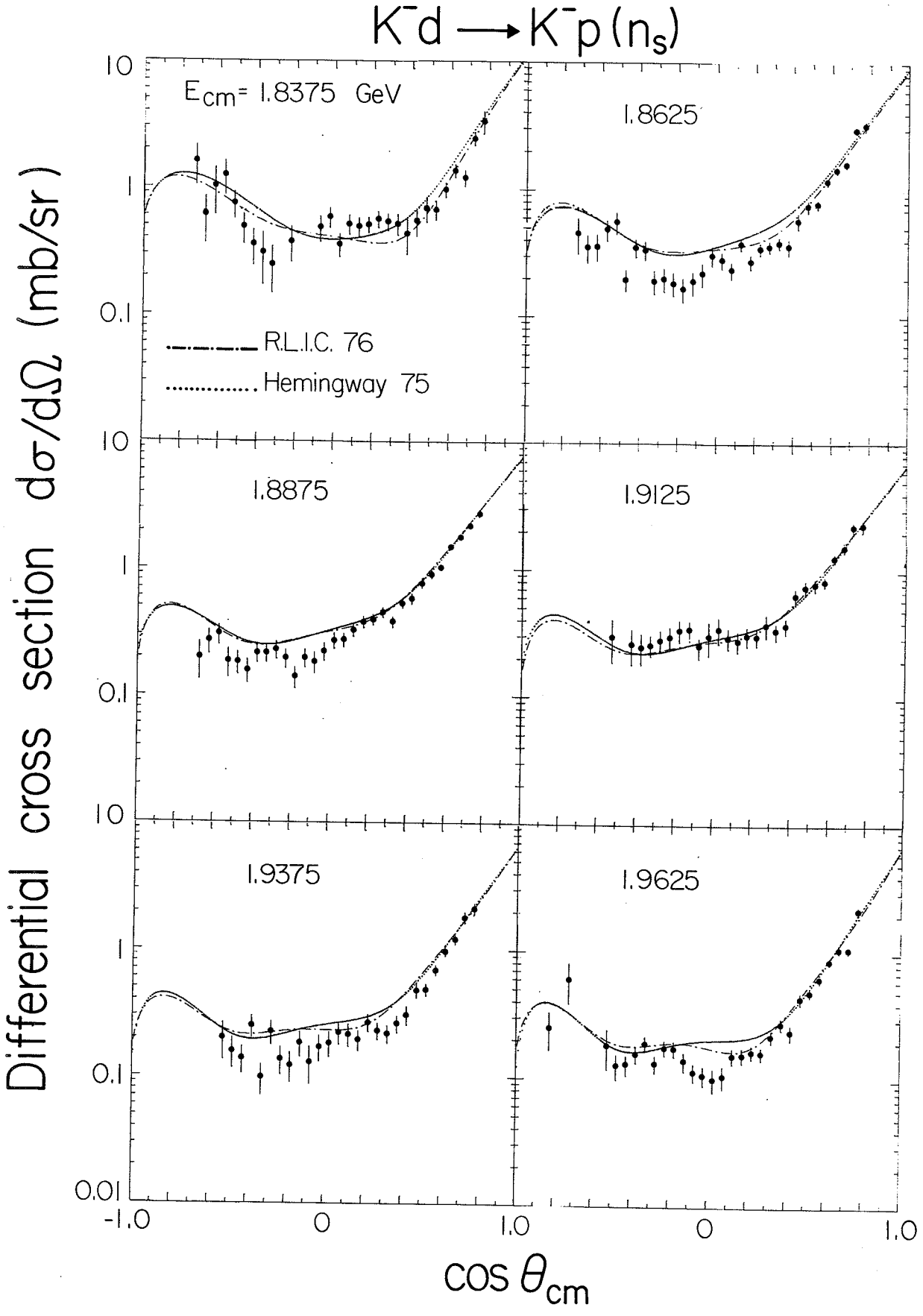
$K^-d \rightarrow K^-p(n_s)$
E_{cm}= 1.8375 GeV
1.8625
1.8875
1.9125
1.9375
1.9625
R.L.I.C. 76
Hemingway 75
Differential cross section $d\sigma/d\Omega$ (mb/sr)
$\cos\theta_{cm}$
10
1
0.1
0.01
-1.0
0
1.0

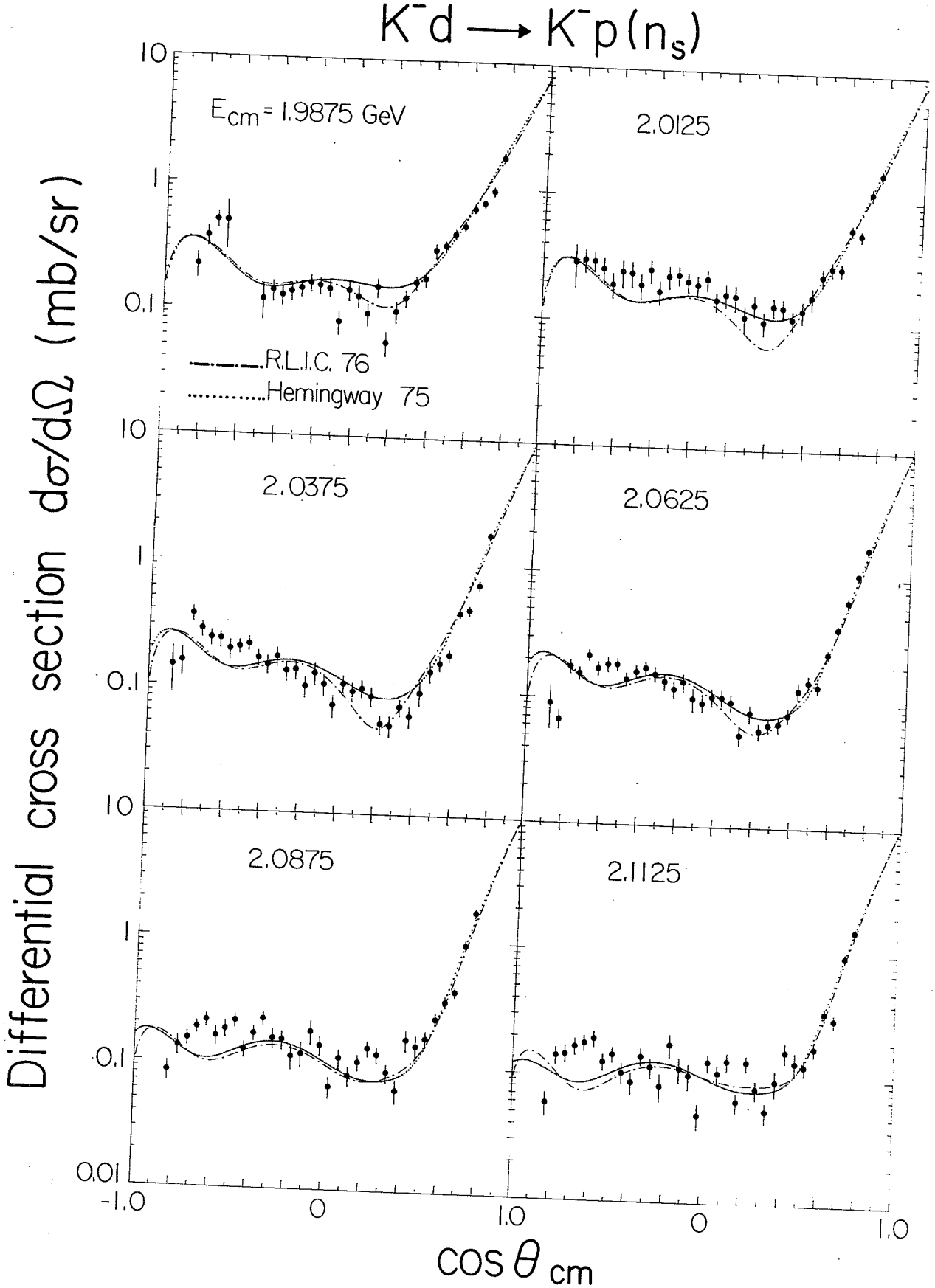
K⁻d ⟶ K⁻p(n_s)
E_cm = 1.9875 GeV
2.0125
2.0375
2.0625
2.0875
2.1125
R.L.I.C. 76
Hemingway 75
Differential cross section dσ/dΩ (mb/sr)
cos θ cm
10
1
0.1
0.01
-1.0
0
1.0

Fig. 3(b)

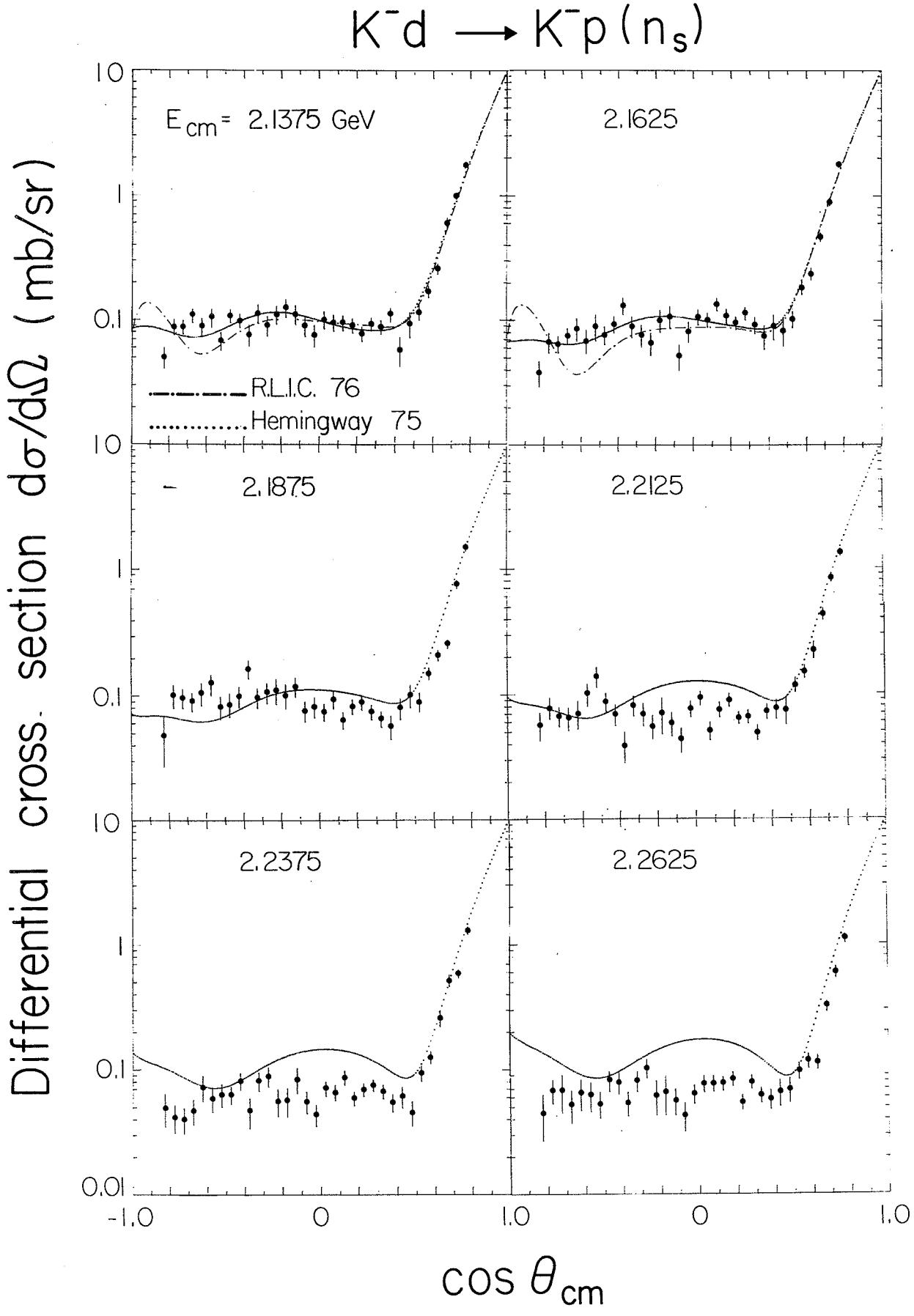
K⁻d → K⁻p(n_s)
E_cm = 2.1375 GeV
2.1625
2.1875
2.2125
2.2375
2.2625
R.L.I.C. 76
Hemingway 75
Differential cross. section dσ/dΩ (mb/sr)
cos θ_cm
10
1
0.1
0.01
-1.0
0
1.0

Fig. 3(c)

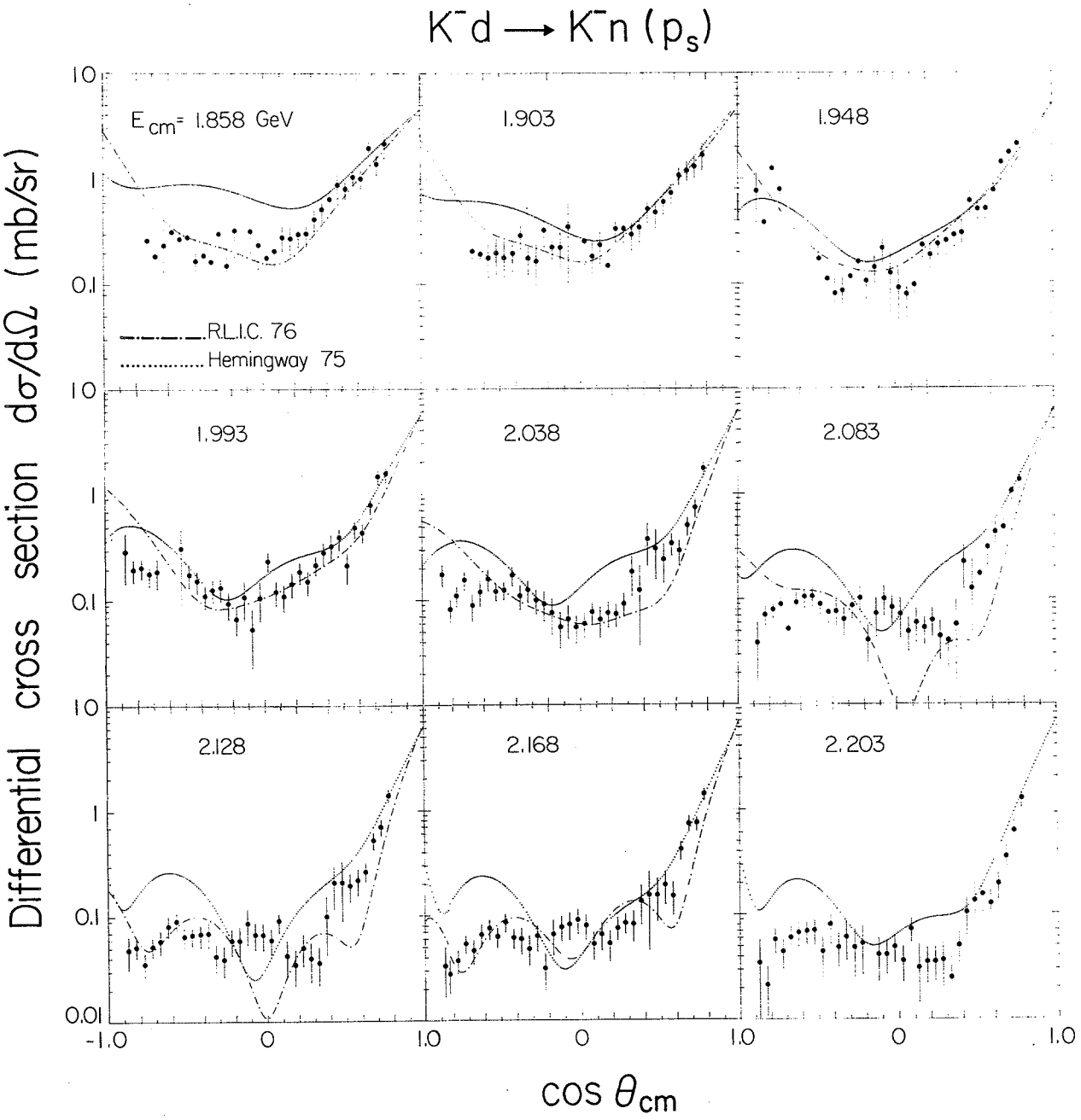
K⁻d ⟶ K⁻n (p_s)
E_cm= 1.858 GeV
1.903
1.948
R.L.I.C. 76
Hemingway 75
1.993
2.038
2.083
2.128
2.168
2.203
Differential cross section dσ/dΩ (mb/sr)
cos θ_cm
10
1
0.1
0.01
-1.0
0
1.0

Fig. 4(a)

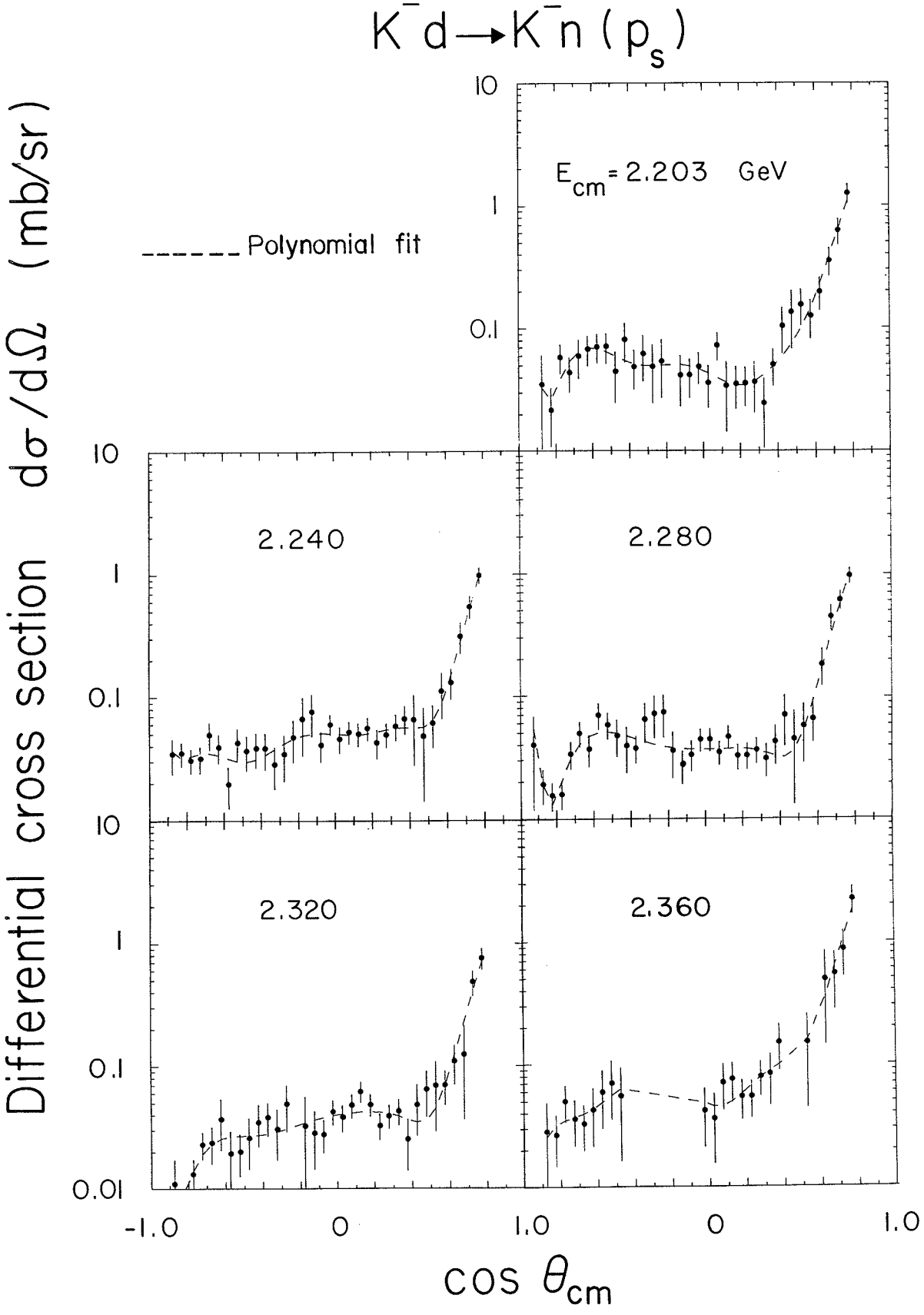
$K^- d \rightarrow K^- n\,(p_s)$
Differential cross section $d\sigma/d\Omega$ (mb/sr)
E_{cm} = 2.203 GeV
Polynomial fit
2.240
2.280
2.320
2.360
10
1
0.1
0.01
-1.0
0
1.0
cos θ_{cm}

Fig. 4(b)

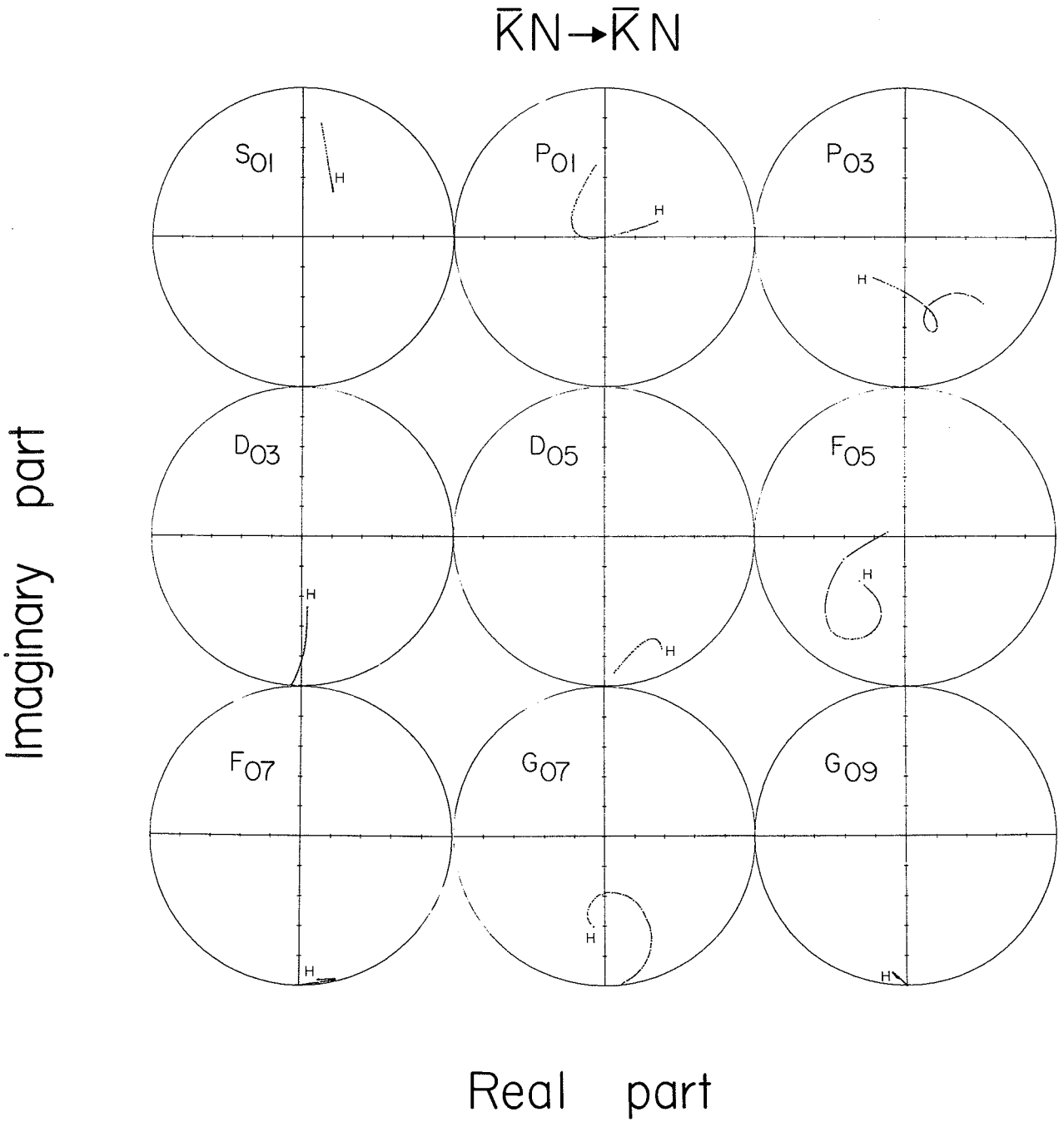

CERN-CAEN 76 phase shifts

Fig. 5(a)

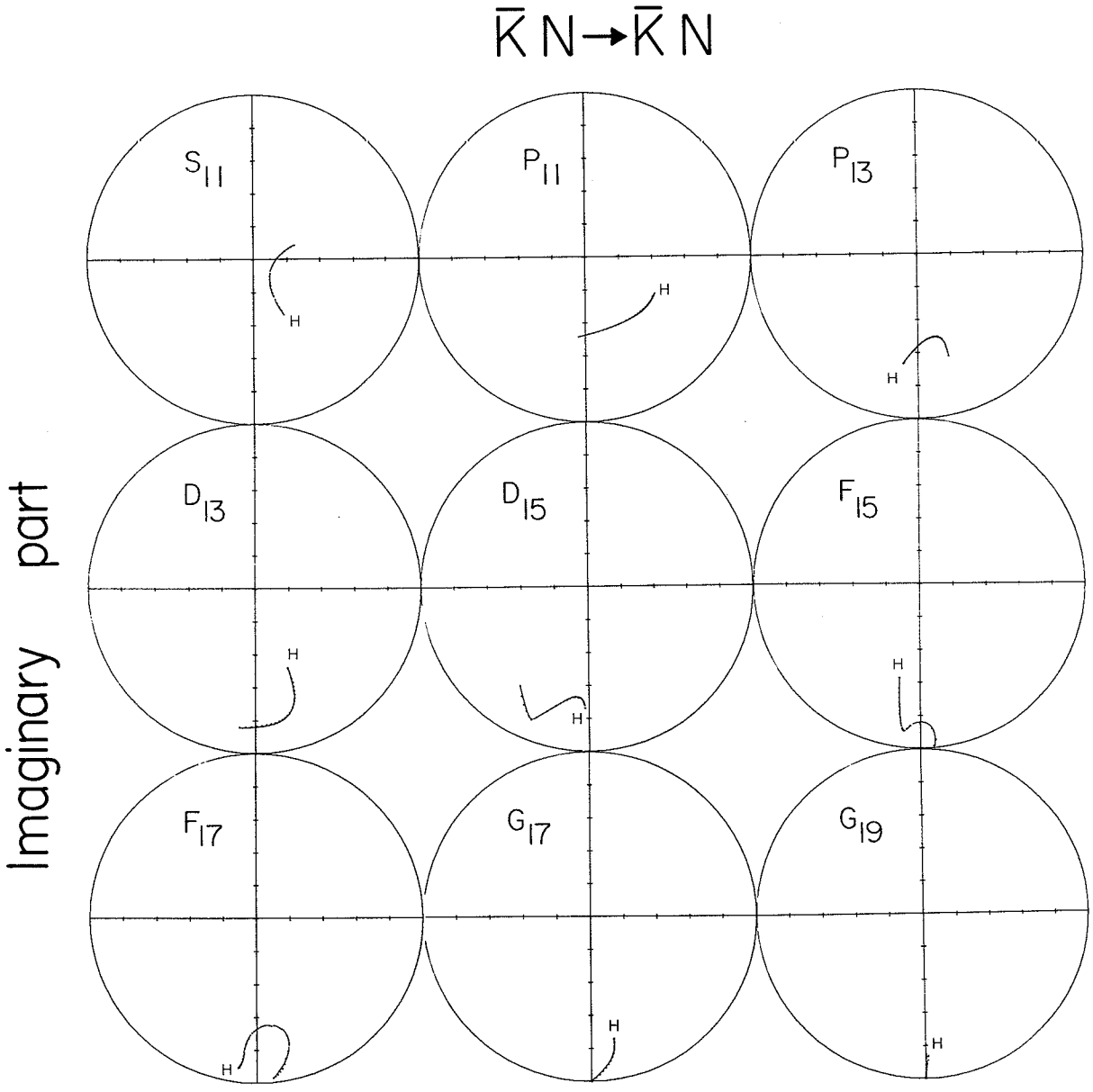

CERN-CAEN 76 phase shifts

Fig. 5(b)

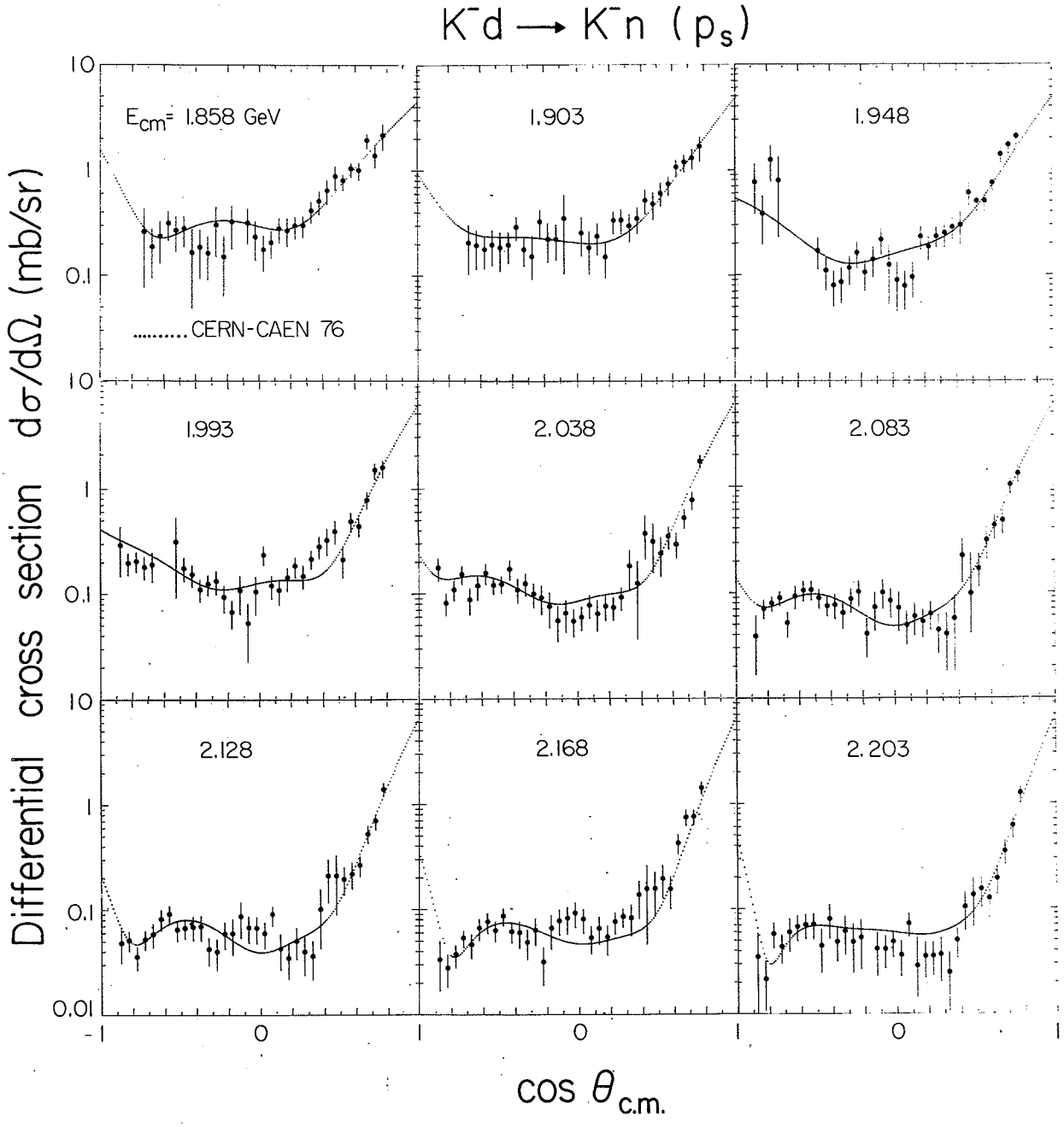
K⁻d → K⁻n (p_s)
E_cm= 1.858 GeV
1.903
1.948
.....CERN-CAEN 76
1.993
2.038
2.083
2.128
2.168
2.203
Differential cross section dσ/dΩ (mb/sr)
cos θ c.m.

Fig. 6

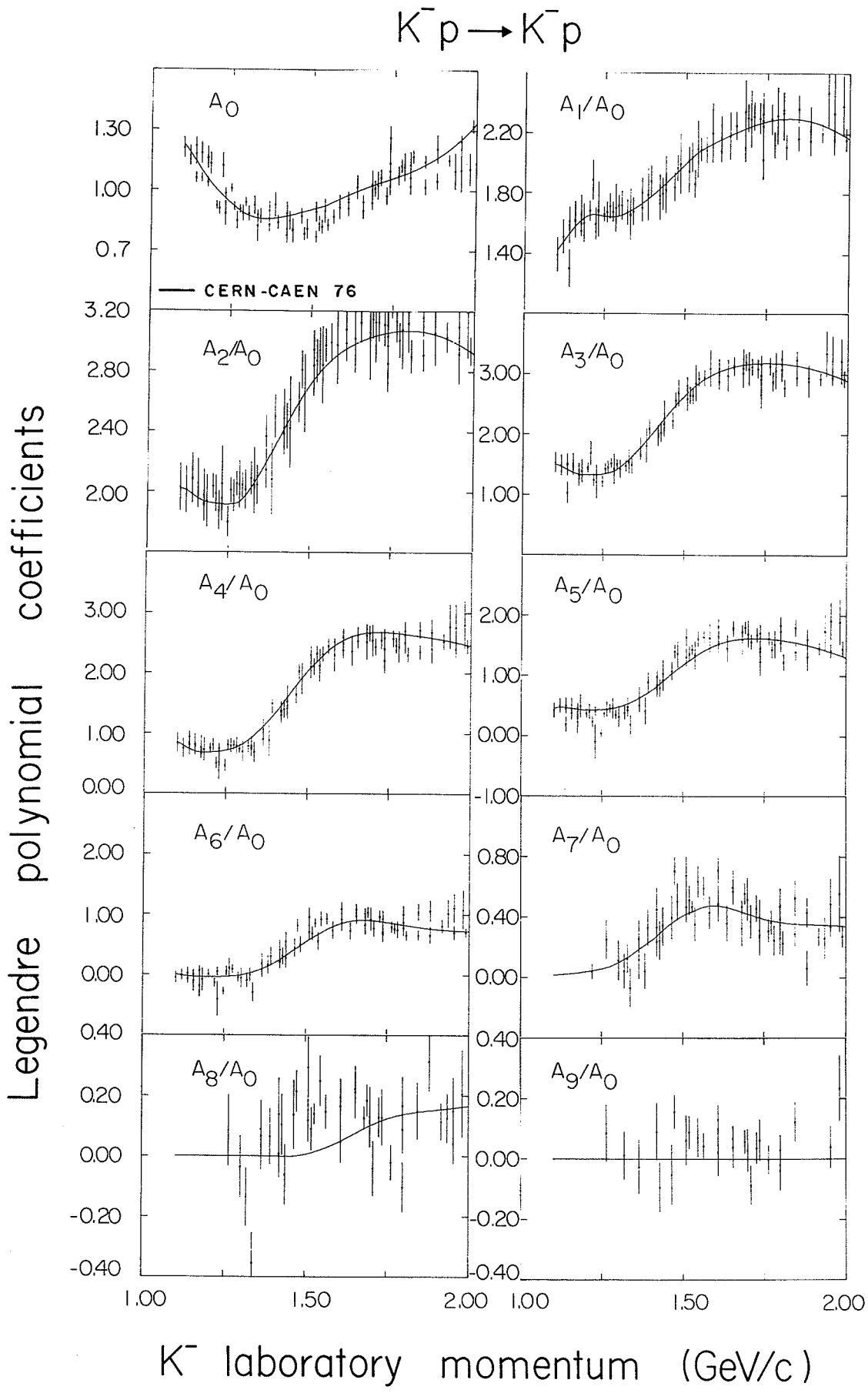
$K^-p \rightarrow K^-p$
A_0
A_1/A_0
A_2/A_0
A_3/A_0
A_4/A_0
A_5/A_0
A_6/A_0
A_7/A_0
A_8/A_0
A_9/A_0
CERN-CAEN 76
Legendre polynomial coefficients
K^- laboratory momentum (GeV/c)

Fig. 7(a)

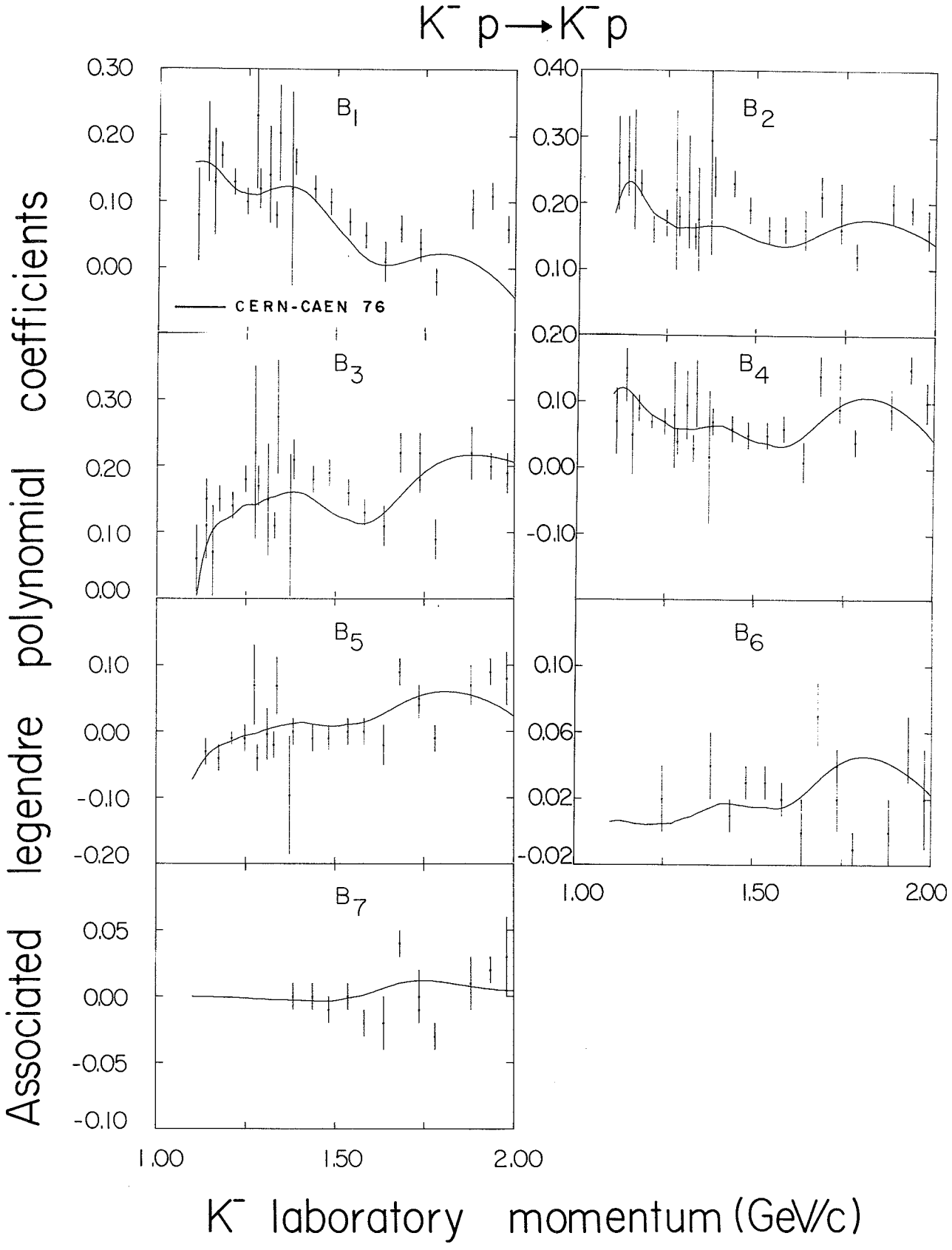
K⁻ p → K⁻ p
Associated legendre polynomial coefficients
B1
B2
B3
B4
B5
B6
B7
CERN-CAEN 76
0.30
0.20
0.10
0.00
0.40
0.30
0.20
0.10
0.20
0.10
0.00
-0.10
0.30
0.20
0.10
0.00
0.10
0.00
-0.10
-0.20
0.10
0.06
0.02
-0.02
0.05
0.00
-0.05
-0.10
1.00
1.50
2.00
K⁻ laboratory momentum (GeV/c)

Fig. 7(b)

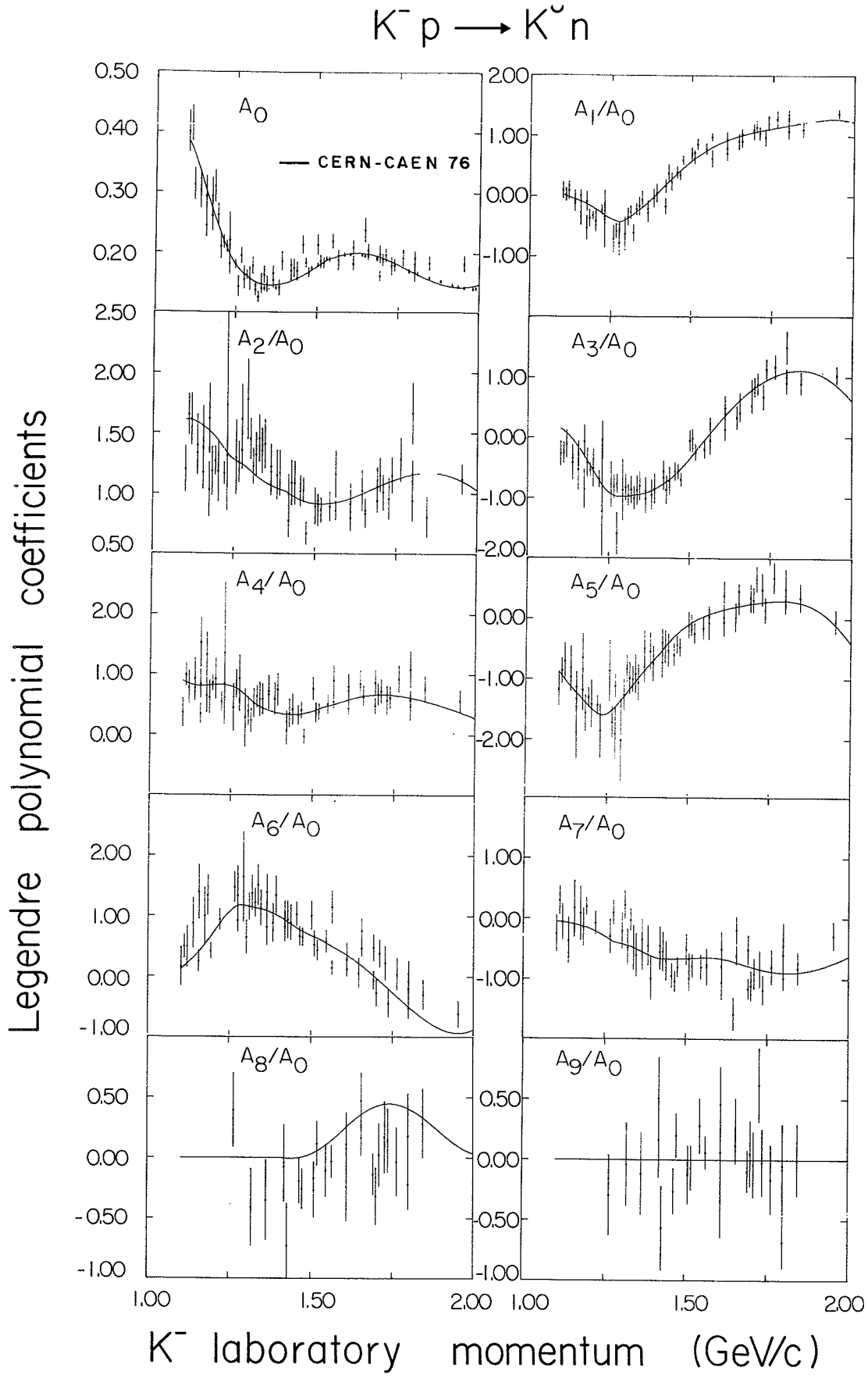
K⁻p ⟶ K°n
A0
— CERN-CAEN 76
A1/A0
A2/A0
A3/A0
A4/A0
A5/A0
A6/A0
A7/A0
A8/A0
A9/A0
Legendre polynomial coefficients
K⁻ laboratory momentum (GeV/c)

Fig. 7(c)

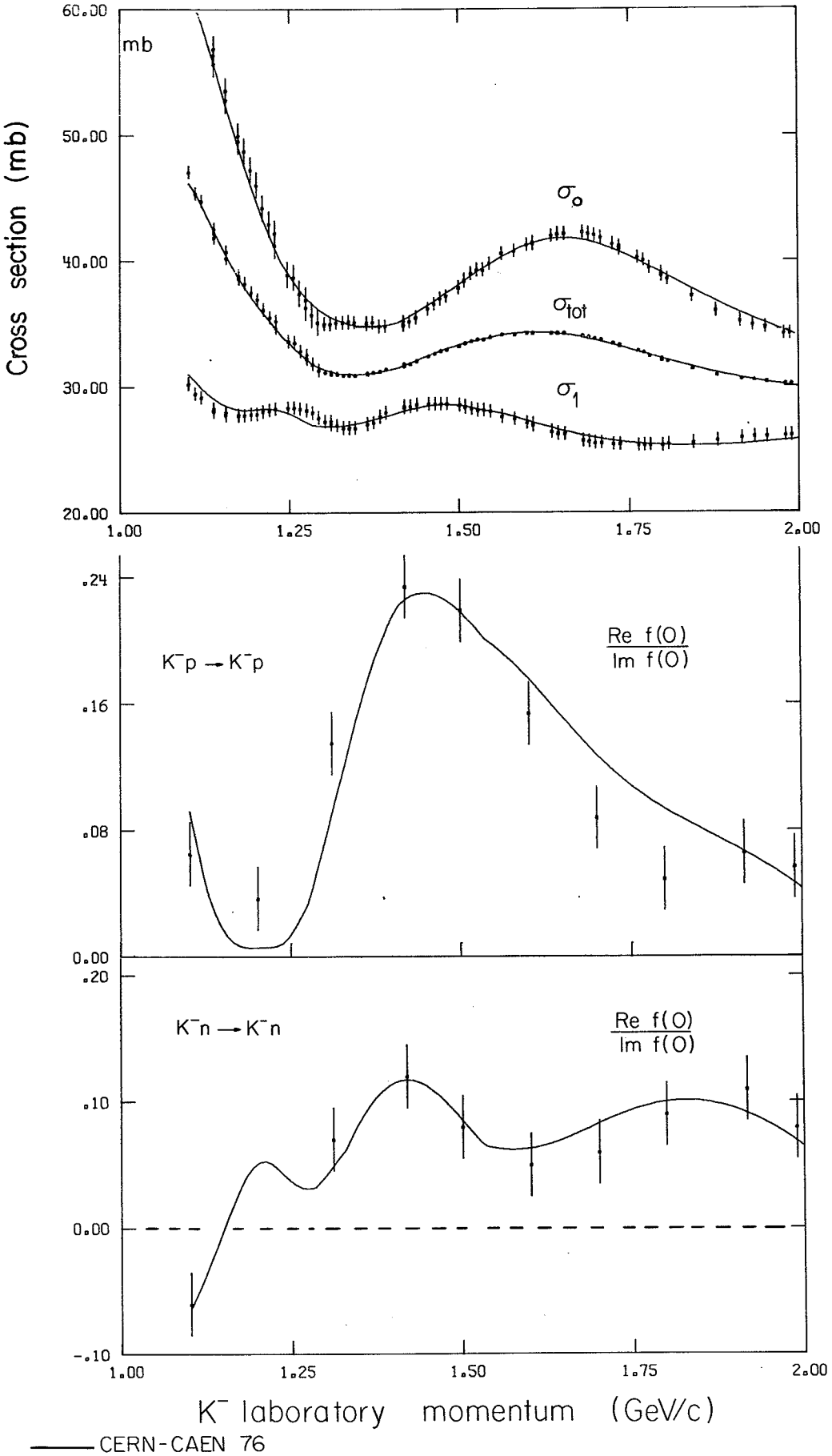
Cross section (mb)
mb
60.00
50.00
40.00
30.00
20.00
σ_o
σ_{tot}
σ_1
1.00
1.25
1.50
1.75
2.00
.24
.16
.08
0.00
$K^-p \rightarrow K^-p$
$\frac{\text{Re } f(0)}{\text{Im } f(0)}$
.20
.10
0.00
-.10
$K^-n \rightarrow K^-n$
$\frac{\text{Re } f(0)}{\text{Im } f(0)}$
K^- laboratory momentum (GeV/c)
CERN-CAEN 76

Fig. 8